

Pipeline thickness estimation using the dispersion of higher-order SH guided waves

Zhengchen Dai(代政辰), Jinxia Liu(刘金霞), Yunfei Long(龙云飞), Jianhai Zhang(张建海), Tribikram Kundu, and Zhiwen Cui(崔志文)

Citation: Chin. Phys. B, 2024, 33 (**7**): 074301. DOI: 10.1088/1674-1056/ad3033
Journal homepage: http://cpb.iphy.ac.cn; http://iopscience.iop.org/cpb

What follows is a list of articles you may be interested in

Experimental realization of fractal fretwork metasurface for sound anomalous modulation

Jiajie He(何佳杰), Shumeng Yu(于书萌), Xue Jiang(江雪), and Dean Ta(他得安)
Chin. Phys. B, 2024, 33 (**5**): 054301. DOI: 10.1088/1674-1056/ad2dcd

Sensing the heavy water concentration in an H_2O—D_2O mixture by solid—solid phononic crystals

Mohammadreza Rahimi and Ali Bahrami
Chin. Phys. B, 2024, 33 (**4**): 044301. DOI: 10.1088/1674-1056/ad0bf5

Effects of confining pressure and pore pressure on multipole borehole acoustic field in fluid-saturated porous media

Zhi-Qiang Zhao(赵志强), Jin-Xia Liu(刘金霞), Jian-Yu Liu(刘建宇), and Zhi-Wen Cui(崔志文)
Chin. Phys. B, 2024, 33 (**1**): 014301. DOI: 10.1088/1674-1056/acf9e6

Acoustic propagation uncertainty in internal wave environments using an ocean-acoustic joint model

Fei Gao(高飞), Fanghua Xu(徐芳华), Zhenglin Li(李整林), Jixing Qin(秦继兴), and Qinya Zhang(章沁雅)
Chin. Phys. B, 2023, 32 (**3**): 034302. DOI: 10.1088/1674-1056/ac89dc

Single SH guided wave mode generation method for PPM EMATs

Guo-Fu Zhai(翟国富), Yong-Qian Li(李永虔)
Chin. Phys. B, 2020, 29 (**5**): 054303. DOI: 10.1088/1674-1056/ab81f8

Pipeline thickness estimation using the dispersion of higher-order SH guided waves

Zhengchen Dai(代政辰)[1], Jinxia Liu(刘金霞)[1,†], Yunfei Long(龙云飞)[1], Jianhai Zhang(张建海)[2], Tribikram Kundu[3,4], and Zhiwen Cui(崔志文)[1,5,‡]

[1] *Department of Acoustics and Microwave Physics, College of Physics, Jilin University, Changchun* 130012, *China*
[2] *School of Mechanical and Aerospace Engineering, Jilin University, Changchun* 130025, *China*
[3] *Department of Civil and Architectural Engineering and Mechanics, University of Arizona, Tucson, Arizona* 85721, *USA*
[4] *College of Aerospace and Mechanical Engineering, University of Arizona, Tucson, AZ* 85721, *USA*
[5] *State Key Laboratory of Acoustics, Institute of Acoustics, Chinese Academy of Sciences, Beijing* 100190, *China*

(Received 11 December 2023; revised manuscript received 29 February 2024; accepted manuscript online 5 March 2024)

Thickness measurement plays an important role in the monitoring of pipeline corrosion damage. However, the requirement for prior knowledge of the shear wave velocity in the pipeline material for popular ultrasonic thickness measurement limits its widespread application. This paper proposes a method that utilizes cylindrical shear horizontal (SH) guided waves to estimate pipeline thickness without prior knowledge of shear wave velocity. The inversion formulas are derived from the dispersion of higher-order modes with the high-frequency approximation. The waveform of the example problems is simulated using the real-axis integral method. The data points on the dispersion curves are processed in the frequency domain using the wave-number method. These extracted data are then substituted into the derived formulas. The results verify that employing higher-order SH guided waves for the evaluation of thickness and shear wave velocity yields less than 1% error. This method can be applied to both metallic and non-metallic pipelines, thus opening new possibilities for health monitoring of pipeline structures.

Keywords: pipeline wall thickness, higher-order modes, SH guided waves, dispersion

PACS: 43.20.+g, 43.40.+s, 43.58.+z, 43.60.+d **DOI:** 10.1088/1674-1056/ad3033

1. Introduction

Pipelines have been widely used to transport crude oil, gas, water and many other vital goods. Because of their long service life, these pipelines are likely to corrode, causing a gradual decrease in their wall thickness. The loss in wall thickness results in reduced structural strength of pipelines. Nondestructive testing (NDT) is an effective way to monitor and evaluate the corrosion conditions of pipelines and hence carry out risk assessments of pipeline failures.[1–3]

Many scholars have proposed nondestructive testing methods for pipeline corrosion. Simonov *et al.*[4] studied nondestructive testing of metal shell corrosion using infrared thermal imaging. Nguyen and Miro.[5] evaluated the residual wall thickness of corroded water pipes using pulsed eddy current data. Chen *et al.*[6] introduced the homotopy analysis method to study the buckling failure of pipes with ideal corrosion defects of different shapes. Numerical examples show that the precise corrosion shape can be obtained. Kiapasha *et al.*[7] measured pipe wall thickness using digital radiography and the three-wavelet method. These efforts have produced satisfactory results.

In recent years, non-destructive testing techniques based on ultrasonic guided waves (UGWs) have gained increasing popularity.[8,9] Many works have focused on guided wave tomography using Lamb waves and SH waves to accurately map the pipe wall thickness, enabling detailed imaging of localized corrosion patches. Notably, the shear horizontal (SH) guided wave exhibits unique propagation characteristics as it propagates between interfaces without waveform conversion and is decoupled from the P-SV wave. Therefore, utilizing SH guided waves to assess the structural health of plates or pipelines is more advantageous. Li[10] employed combined harmonics generated by two longitudinal guided waves in pipelines to precisely locate local degradation and determine its severity. El Mountassir *et al.*[11] utilized ultrasonic guided waves to detect and locate minor corrosion in pipelines. Wang *et al.*[12] simulated pitting detection within pipe interiors using guided waves. Li *et al.*[13] analyzed the propagation characteristics of water-filled steel pipes and flanged joints with respect to guided wave behavior while estimating damage levels. Belanger[14] estimated defect thickness in aluminum plates by leveraging the cutoff properties of higher-order shear horizontal waves. Howard and Cegla investigated interactions between SH_1 and SH_2 modes with defects from guided wave analysis. De Castro Ribeiro *et al.*[15] assessed the defect size by analyzing interactions between SH guided waves and defects, directly benchmarking their method against real-world defect scenarios. Thon *et al.*,[16] employing higher-order SH modes, reconstructed circumferential thickness distribution in steel pipes, even for complex corrosion

†Corresponding author. E-mail: jinxia@jlu.edu.cn
‡Corresponding author. E-mail: cuizw@jlu.edu.cn

© 2024 Chinese Physical Society and IOP Publishing Ltd

conditions. Cui *et al.*[17] used d_{15} piezoelectric transducers to excite SH_2 mode, and constructed a damage-detection method for thick plate structures based on the reconstruction algorithm for probabilistic inspection of damage (RAPID). Their work broadens the application of SH guided waves in thick plate structures and complex structures. Sun *et al.*[18] proposed a physics-informed deep neural network based on a unidirectional oblique-focusing (UOF) high-frequency, high-order shear horizontal guided wave electromagnetic acoustic transducer (EMAT) to quantify microcrack defects more accurately. Nascimento *et al.* investigated which SH modes are more appropriate for circumferential inspection of a coated pipe of interest. The results of the study show that for different frequency-thickness modes, the selection of appropriate operating modes is crucial. Dixon *et al.*[19] proposed a method to retrieve the thickness based on the phase velocity and group velocity extracted from SH guided wave signals without knowledge of the body wave velocity. By solving the parameters of the Fourier transform of SH_0 and SH_1 signals, an error accuracy of 1% was obtained. However, since their method only used single higher-order mode information, they needed to excite the signal twice to obtain the desired parameters.

However, despite the favorable outcomes achieved by all the aforementioned methods, there remains a scarcity of techniques for the efficient detection of tube wall thickness using SH guided waves over long distances. In this paper, we propose a novel approach that is suitable for determining the average value of pipe wall thickness across extensive distances by simultaneously estimating the thickness, shear wave velocity, and mode order via any two adjacent higher-order dispersion curves. Compared to the widely used ultrasonic pulse velocity method (UPV),[20] our method eliminates the need for prior knowledge of wave velocity in the material. Furthermore, it automatically identifies excited modes, even without corresponding theoretical dispersion curves. Additionally, our method is applicable to both metal and non-metal materials, thereby offering a broad range of potential applications.

The content of this paper is organized as follows: Section 2 provides an elaborate description of the SH wave field in pipelines; Section 3 presents inversion formulas for two different cases involving thickness estimation; Section 4 outlines the solution and inversion process; Section 5 gives the results and discussion; finally, conclusions are drawn in Section 6.

2. SH wave field in pipeline

The pipeline model is a cylindrical single-layer structure, as shown in Fig. 1. The inside and outside of the cylindrical single-layer elastic medium are fluids. An annular shear source is simulated by a small ring, which is perfectly attached to the outer surface, and can efficiently excite SH guided waves and transmit them to the pipeline.

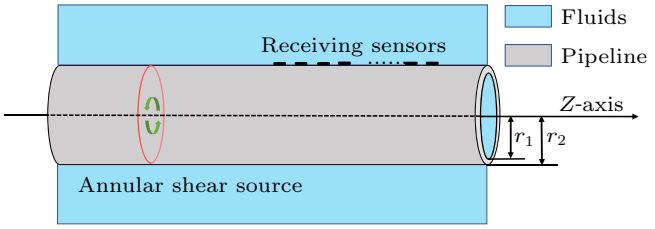


Fig. 1. A schematic diagram of the pipeline model.

The inner diameter and the outer diameter of the pipeline are r_1 and r_2, respectively. The governing equation in terms of χ, the shear wave potential is

$$\nabla^2\chi + \frac{1}{c_s^2}\frac{\partial^2\chi}{\partial t^2} = 0, \tag{1}$$

where c_s is the shear wave speed in the elastic medium. Since the whole system is axisymmetric, it can be easily solved in the cylindrical coordinate system. In this coordinate system, the tangential stress component at the inner surface ($r = r_1$) is 0. The tangential stress component at the outer surface ($r = r_2$) is equal to the annular shear transducer generated stress. Therefore, the boundary conditions can be expressed as follows:

$$\sigma_{r\theta} = 0 \quad \text{at} \quad r = r_1, \tag{2}$$

$$\sigma_{r\theta}(r,z,t) = \delta(r-r_2)\delta(z)f(t) \quad \text{at} \quad r = r_2, \tag{3}$$

where $f(t)$ is the time dependence of the acoustic source. Using the separation of variables, the shear wave potential χ can be expressed in the following Fourier integral form:

$$\chi(r,z,t) = \frac{1}{(2\pi)^2}\int_{-\infty}^{\infty}\int_{-\infty}^{\infty}[A_1 I_0(mr) + B_1 K_0(mr)] \times F(\omega)\,\mathrm{e}^{\mathrm{j}k_z z}\,\mathrm{e}^{-\mathrm{j}\omega t}\,\mathrm{d}k_z\,\mathrm{d}\omega, \tag{4}$$

$$m^2 = k_z^2 - k_s^2, \tag{5}$$

where k_z is the axial wave number, ω is the angular frequency, $I_0(z)$ and $K_0(z)$ are the modified Bessel functions of the first and the second kinds, respectively, A_1 and B_1 are the unknown coefficients to be solved, and $F(\omega)$ is the frequency domain representation of the acoustic source function. The relationship between the tangential displacement u_θ and the tangential stress component $\sigma_{r\theta}$ is as follows:

$$\sigma_{r\theta} = \mu\left(-\frac{u_\theta}{r} + \frac{\partial u_\theta}{\partial r}\right), \tag{6}$$

where μ is the shear modulus of the elastic medium. Satisfying the two boundary conditions, the following matrix equation can be obtained:

$$\begin{pmatrix} a_{11} & a_{12} \\ a_{21} & a_{22} \end{pmatrix}\begin{pmatrix} A_1 \\ B_1 \end{pmatrix} = \begin{pmatrix} \sigma_{r\theta}(z) \\ 0 \end{pmatrix}. \tag{7}$$

For propagation of the guided wave along the traction-free pipe, the necessary and sufficient condition is that the determinant of the coefficient matrix of Eq. (7) is equal to zero. It gives the dispersion equation

$$D(k_z, \omega) = 0. \tag{8}$$

The roots obtained by solving this equation are the axial wave numbers k_z at various frequency values ω. Thus, for propagation of guided waves in the axial direction in a cylindrical single-layered elastic medium, Eq. (8) gives the following equation:

$$\begin{vmatrix} -\mu m^2 I_2(mr_2) & -\mu m^2 K_2(mr_2) \\ -\mu m^2 I_2(mr_1) & -\mu m^2 K_2(mr_1) \end{vmatrix} = 0. \tag{9}$$

The equation above is the characteristic equation of the SH wave field excited by a ring-shaped shear transducer. In many industrial applications, the radius of the pipe is much larger than its thickness.[21] This geometric structure can be simplified using the approximate theory for the infinite outer diameter of the pipeline. When the arguments of the modified Bessel functions in Eq. (9) become infinite, the dispersion equation can be obtained as follows:

$$\frac{\omega^2}{c_s^2} - \frac{\omega^2}{c^2} = \left(\frac{n\pi}{h}\right)^2, \tag{10}$$

where $h = r_2 - r_1$, c_s is the shear wave speed in the elastic medium. From Eq. (19) we can see that the cylindrical single elastic layer evolves into an elastic plate. This analytical expression is consistent with the SH wave dispersion equation for a plate.[22] It should be noted that the pipe-to-plate approximation is reasonable only when the thickness to outer diameter ratio of the pipe, i.e., the standard dimension ratio (SDR), is less than 10%–15%.[23]

3. Inversion formulas for thickness

The dispersion curves of SH guided waves, as shown in Fig. 2(a), show that there are several modes in a cylindrical single elastic layer. The inversion formulas are acquired from the dispersion relationship. In practice, setting the appropriate frequency bandwidth of the excitation signal and the spatial bandwidth of the sensor can stimulate the multi-mode phenomenon.[24,25] However, at a fixed frequency, higher-order modes cannot propagate if the thickness is below the cut-off thickness $h_{\text{cut-off}} = nc_s/(2f)$.[26,27] The model proposed in this paper does not consider scattering and mode conversion of SH guided waves; therefore, for a certain frequency, at least two modes can be complete dispersion curves. The possible multimodal phenomena can be classified under two groups based on whether the adjacent dispersion curves have overlapping phase velocity values, as shown in Figs. 2(b) and 2(c).

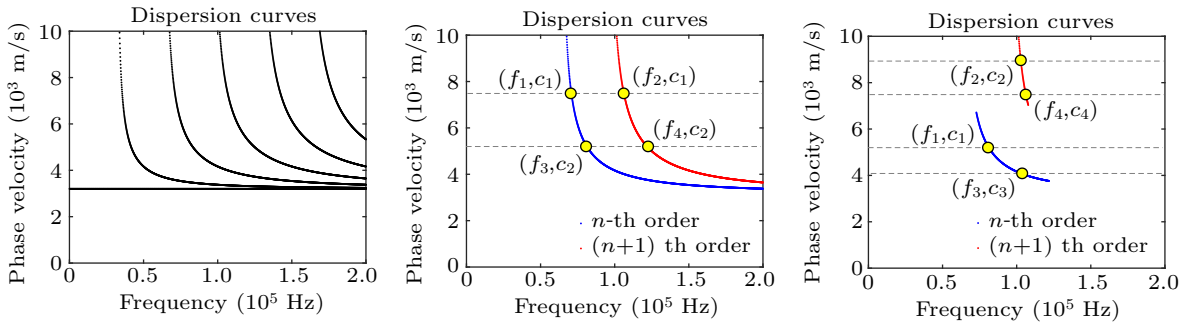


Fig. 2. Phase velocity dispersion curves of SH guided waves in steel plate ($C_s = 3200$ m/s, $h = 0.05$ m). (a) Dispersion curves obtained from Eq. (1). (b) Case I: adjacent dispersion curves with overlapped phase velocity values; and (c) case II: adjacent dispersion curves without overlapped phase velocity values.

It can be observed in Fig. 2(b) that in higher-order adjacent curves, there are data points with the same phase velocity: we named this condition case I. The overlapping velocity has the advantage of efficient and concise inversion formulas. Case II in Fig. 2(c) is discussed in Subsection 3.2. We will produce another set of formulas for this case.

3.1. Case I

Let the coordinates of the two points in the n-th order frequency curve be (f_1,c_1), (f_3,c_2), and the coordinates of the two points on the $(n+1)$-th order frequency curve be (f_2,c_1), (f_4,c_2).

$$\frac{\omega_1^2}{c_s^2} - \frac{\omega_1^2}{c_1^2} = \left(\frac{n\pi}{h}\right)^2, \tag{11a}$$

$$\frac{\omega_3^2}{c_s^2} - \frac{\omega_3^2}{c_2^2} = \left(\frac{n\pi}{h}\right)^2, \tag{11b}$$

$$\frac{\omega_2^2}{c_s^2} - \frac{\omega_2^2}{c_1^2} = \left(\frac{(n+1)\pi}{h}\right)^2, \tag{12a}$$

$$\frac{\omega_4^2}{c_s^2} - \frac{\omega_4^2}{c_2^2} = \left(\frac{(n+1)\pi}{h}\right)^2. \tag{12b}$$

From Eqs. (11a) and (12a), the order n can be obtained as

$$n = 1 \Big/ \left(\frac{f_2}{f_1} - 1\right). \tag{13}$$

From Eqs. (12a) and (12b), the shear transverse wave velocity can be obtained by

$$c_s = \sqrt{\frac{\omega_2^2 - \omega_4^2}{\frac{\omega_2^2}{c_1^2} - \frac{\omega_4^2}{c_2^2}}} = \sqrt{\frac{f_2^2 - f_4^2}{\frac{f_2^2}{c_1^2} - \frac{f_4^2}{c_2^2}}}. \tag{14}$$

Then, by substituting c_s and n into Eq. (12a), the thickness h can be solved as

$$h = (n+1) \Big/ \left(2\sqrt{\frac{f_2^2}{c_s^2} - \frac{f_2^2}{c_2^2}}\right). \tag{15}$$

3.2. Case II

Let the coordinates of the two points in the n-th order curve be (f_1, c_1), (f_3, c_3), and the coordinates of the two points on the $(n+1)$-th order curve be (f_2, c_2), (f_4, c_4).

$$\frac{\omega_1^2}{c_s^2} - \frac{\omega_1^2}{c_1^2} = \left(\frac{n\pi}{h}\right)^2, \tag{16a}$$

$$\frac{\omega_3^2}{c_s^2} - \frac{\omega_3^2}{c_3^2} = \left(\frac{n\pi}{h}\right)^2, \tag{16b}$$

$$\frac{\omega_2^2}{c_s^2} - \frac{\omega_2^2}{c_2^2} = \left(\frac{(n+1)\pi}{h}\right)^2, \tag{17a}$$

$$\frac{\omega_4^2}{c_s^2} - \frac{\omega_4^2}{c_4^2} = \left(\frac{(n+1)\pi}{h}\right)^2. \tag{17b}$$

First, c_s is calculated in the same way as Eq. (12) in Subsection 3.1. Next, consider the dispersion equations of any point in each adjacent curve. By comparing Eqs. (16a) and (17a), the order n can be obtained as

$$n = 1 \Big/ \left(\frac{f_2 c_1}{f_1 c_2}\sqrt{\frac{c_2^2 - c_s^2}{c_1^2 - c_s^2}} - 1\right). \tag{18}$$

Then, the thickness h can be solved similarly to Eq. (15). For case II, one must calculate c_s, n and thickness h in progressive order, while c_s and n can be solved as in case I.

4. Inversion process

So far, we have derived, theoretically, the frequency dispersion equation and given two analytical inversion expressions from the frequency dispersion equation. From Eqs. (13)–(15) and (18), it can be seen that the inversion results for transverse wave velocity, order, and thickness can be calculated by obtaining the frequency–velocity data points of the SH guided waves and substituting them into the inversion equations. Using the frequency–wave-number method to extract the dispersion curves can obtain the distribution of the wave-field energy at different frequencies, which is applicable to the model in this paper. In this section, we simulate the orthotropic wave field and use the frequency–wave-number method to pick up the dispersion characteristic data points to verify the feasibility of the final inversion results.

4.1. Full-wave simulation

Here, an example is given to show the specific inversion process. The specific parameter settings are shown in Table 1. Place the full-wave sound field sensors close to the outer surface of the cylindrical single-layer elastic medium. The transient waveform of the shear displacement at the outer surface can be calculated using the real-axis integration method. From the displacement expression $u_\theta = -\partial\chi/\partial r$, we know that once the unknown coefficients A_1, B_1 and the source function are determined by Eq. (7), we can obtain transient waveforms by using a discrete wave-number integration. When calculating the full waveform in the time domain, the cosine envelope pulse is selected as the acoustic source function

$$f(t) = \begin{cases} \dfrac{1}{2}\left[1 + \cos\dfrac{2\pi}{T}\left(t - \dfrac{T}{2}\right)\right]\cos 2\pi f_0\left(t - \dfrac{T}{2}\right), & 0 \le t \le T, \\ 0, & t \le 0,\ t \ge T, \end{cases} \tag{19}$$

where f_0 is the center frequency of the acoustic source, and T is the pulse width of the source. The numerical value of parameter T is inversely proportional to the spectral width for the corresponding model. Taking the parameters given in Table 1 as an example, the -3 dB spectral bandwidth of the model is 302.9 kHz–407.1 kHz. The waveform diagram of each channel is shown in Fig. 3.

Table 1. The parameters of the example.

Pipeline thickness h (mm)	8.38
Standard dimension ratio (SDR)	2.59%
Source center frequency f_0 (kHz)	400
Sound source pulse width T (s)	7.5×10^{-6}
Number of sensors	32
The distance between the first sensor and the sound source (m)	0.01
Spacing between sensors (m)	0.008

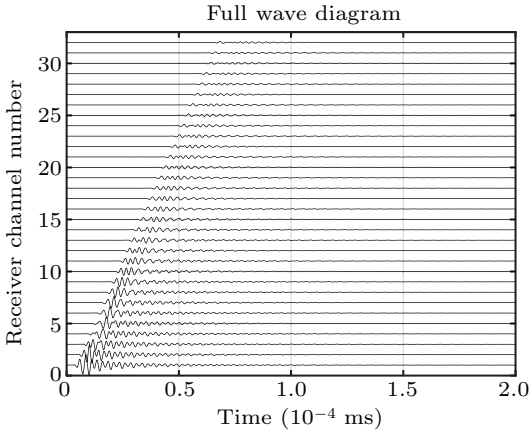


Fig. 3. The array waveforms diagram.

4.2. The 2D Fourier transform

In this paper, the frequency–wave-number method for processing signals of wave structures in time and space do-

mains is chosen.

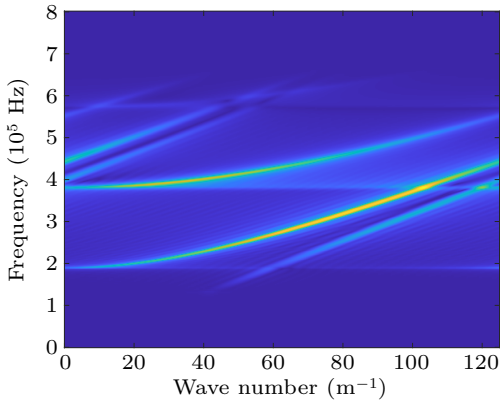


Fig. 4. The shear displacements in the frequency–wavenumber domain.

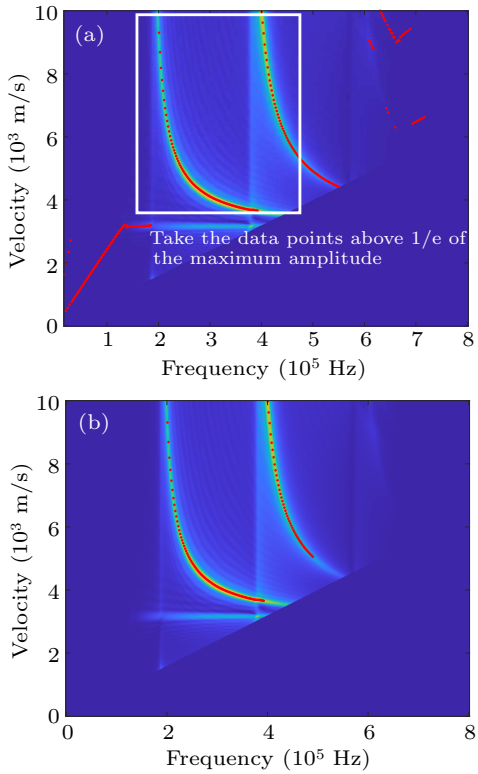


Fig. 5. Energy distribution images of the FFT results. (a) The combination of calculated frequency–velocity points and displacement field; (b) data points obtained by windowing.

Here, two-dimensional (2D) Fourier transform is carried out to transform the shear displacements into the frequency–wave-number domains, as shown in Fig. 4. Then, all the data points are sampled in the frequency–wave-number domain using the relation $v = f/k$ and converted to the frequency–velocity domains, as shown in Fig. 5(a). The relative magnitudes of $\mu_\theta(\omega, c)$ show the relative contributions of different wave modes at that frequency.[2,28,29] For all given frequency points where the peak of the amplitude of the acoustic field occurs, the phase velocity can be determined; the calculated frequency–velocity points are marked in red in Fig. 5(a). To ensure the accuracy of the extracted frequency and velocity points, the amplitude of the data is limited to $\exp(-1)$ of the maximum value of $\mu_\theta(\omega, c)$. The data points obtained by windowing are shown in Fig. 5(b).

We use the adjacent dispersion curves in the corresponding inversion formulas. It is well known that the median is not affected by extreme data and can show the central tendency of the data. To reduce accidental error, the median is taken as the final value for all results. These analytical procedures and the results obtained from them are described in the next section.

5. Results

To verify the feasibility and applicability of the proposed method in this paper, four examples with different materials and thicknesses are selected for further investigation, as shown in Table 2. PVC pipes with a diameter of 315 mm are often used to discharge sanitary sewage.[30] The two types of steel pipes shown in the table are about 50 years old, and some of them are in urgent need of repair. It should be noted that the frequency band has a certain impact on the method proposed in this article. Case I requires a wider frequency band to ensure the excitation of two modal dispersion curves with the same velocity point, while case II can still be applicable in narrow frequency bands. We added a narrow-band comparison group in case II to verify the impact of bandwidth and the applicability of the method.

Table 2. The parameters of four models.

Model	A	B	C	D
Material type	PVC	steel	PVC	steel
Thickness (mm)	9.20	8.38	7.70	9.53
Outer diameter (mm)	315.00	323.80	315.00	323.80
SDR	2.92%	2.59%	2.44%	2.94%
Source center frequency f_0 (kHz)	125	400	155	350
Sound source pulse width T (s)	0.2×10^{-4}	0.75×10^{-4}	0.2×10^{-4}|1.5×10^{-4}	0.1×10^{-4}|0.6×10^{-4}
Number of sensors			32	
The distance between the first sensor and the source (m)			0.01	
Spacing between sensors (mm)	9.2	8.0	7.4	9.1

5.1. Discussion of case I

In this numerical simulation no points with exactly the same velocity were observed on the two adjacent calculated curves. Therefore, we interpolate the low-order original data. The interpolation precision is set as 0.1 m/s; the half of the interpolation precision is given as a limit to judge whether ap-

proximations can be executed. We let the points in the lower-order data, where the velocity is close to the limit value, be equal to the corresponding higher-order velocity. Then, the data are substituted into Eqs. (13)–(15). The results are shown in Fig. 6 and Table 3. Apparently, for models with different materials and different thicknesses, one can obtain satisfactory inversion results for case I.

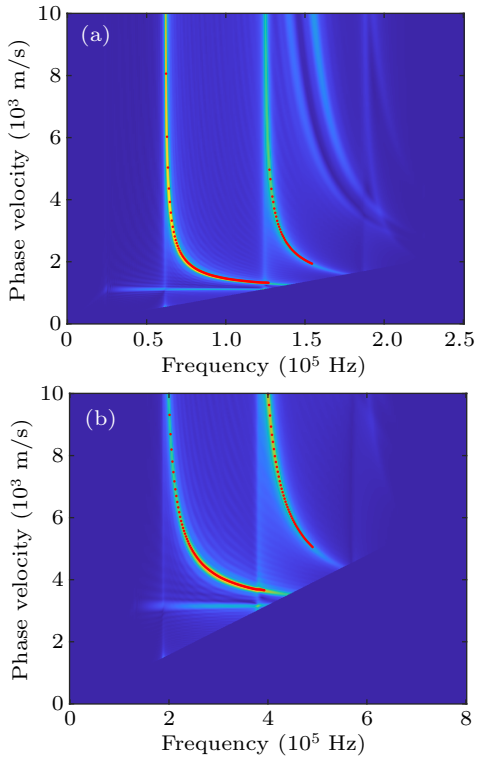


Fig. 6. Energy distribution images from (a) the responses of model A for case I, and (b) the responses of model B in case I.

5.2. Discussion of case II

5.2.1. Wide frequency band

For the wide frequency band, all the data points are extracted and substituted into Eqs. (14), (15) and (18) for ergodic calculation. The results are shown in Fig. 7 and Table 3, which show that the thickness inversion error in case II is lower than that in case I. Obviously, different models have different effects on the inversion results. To investigate the influence of different methods, we adopted the case II processing method for models A and B and conducted calculations for all the original data points. The calculated results are shown in Table 4. In Table 4, we can see that two cases have approximately similar influences on the inversion results. Meanwhile, in case I, the method of case II can be used to further verify the accuracy of the inversion results, providing a double guarantee for the inversion process.

5.2.2. Narrow frequency band

For narrow-band cases, there is a significant reduction in the number of available data points, as shown in Fig. 8, which also leads to an increase in the error of the inversion results, as shown in Table 3. The method proposed in this article is more suitable for broadband excitation, but the results obtained using narrow-band excitation are still within an acceptable error range, fully demonstrating the robustness of this method.

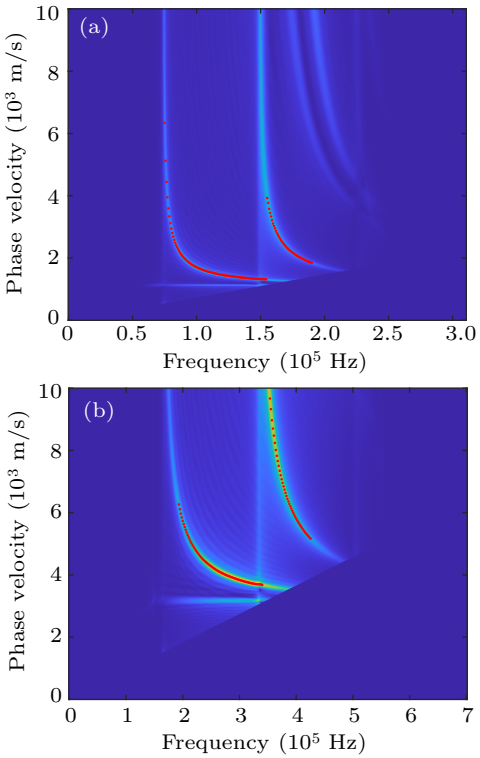


Fig. 7. Energy distribution images from (a) the responses of model C for case II, and (b) the responses of model D for case II.

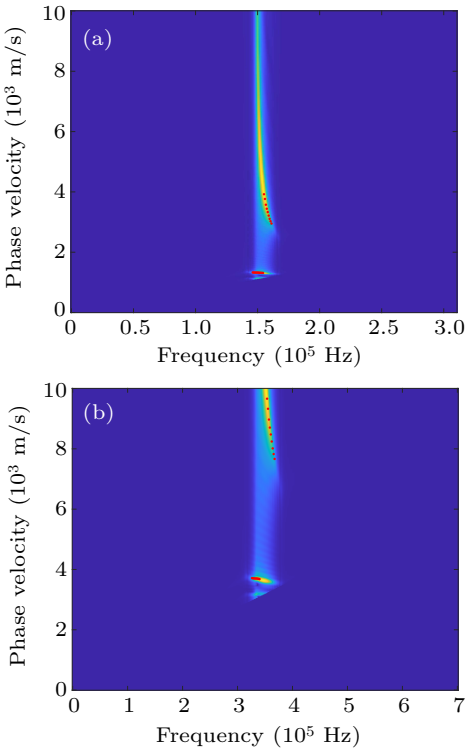


Fig. 8. Energy distribution images from (a) the responses of model C for case II, and (b) the responses of model D for case II.

Table 3. The calculated results of four models.

Material	Inversion parameters	Case 1			Case 2					
					Wide frequency band			Narrow frequency band		
		True value	Calculated value	Error	True value	Calculated value	Error	True value	Calculated value	Error
PVC	C_s (m/s)	1150	1148.92	0.09%	1150	1141.32	0.75%	1150	1166.33	1.42%
	H (mm)	9.20	9.29	0.96%	7.70	7.71	0.12%	7.70	7.84	1.82%
Steel	C_s (m/s)	3200	3166.55	1.05%	3200	3208.02	0.25%	3200	3229.75	0.93%
	H (mm)	8.38	8.37	0.14%	9.53	9.61	0.80%	9.53	9.64	1.17%

Table 4. Comparison of the results of models A and B for different cases.

Material	Inversion parameters	Case 1			Case 2		
		True value	Calculated value	Error	True value	Calculated value	Error
PVC	C_s (m/s)	1150	1148.92	0.09%	1150	1148.45	0.13%
	H (mm)	9.20	9.29	0.96%	9.20	9.28	0.90%
Steel	C_s (m/s)	3200	3166.55	1.05%	3200	3193.59	0.20%
	H (mm)	8.38	8.37	0.14%	8.38	8.45	0.79%

5.3. Model stability in a noisy environment

For practical measurements, background noise is inevitable and ubiquitous. Sometimes it will bring error to the measurement. To discuss the effect of noise on the stability of this method, models A and B with background noise are tested. Gaussian white noise with a signal-to-noise ratio SNR = 20 dB is constructed as a uniform background noise,[31] whichis the limit to obtain sufficient data points for inversion of the thickness value; therefore, here we only show the response under these conditions in Fig. 9.

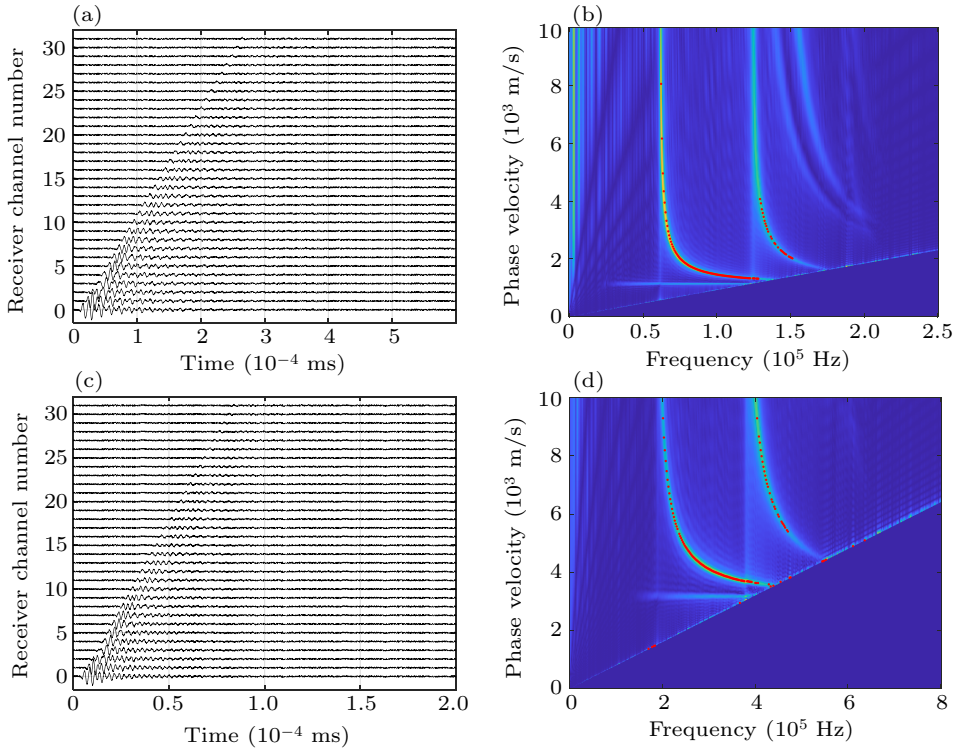


Fig. 9. The responses of model A with background noise: (a) the 32-channel array waveform diagram, and (b) the energy distribution image. The responses of model B with background noise: (c) the 32-channel array waveform diagram, and (d) the energy distribution image.

Table 5. Inversion results under a noisy background.

Material	Inversion parameters	SNR = 20 dB		
		True value	Calculated value	Error
PVC	C_s (m/s)	1150	1149.74	0.02%
	H (mm)	9.20	9.30	1.03%
Steel	C_s (m/s)	3200	3193.24	0.21%
	H (mm)	8.38	8.44	0.77%

Obviously, the number of calculated data points is greatly reduced for the noisy background. The inversion method of case II should be adopted in this model by choosing all the data points. The amount of higher-order data decreased sharply; therefore, using data at high frequency does not mean the results are more accurate. Therefore, we use the n-th order data for inversion and take the average value. The results in Table 5 show that the method is still reliable, even for the condition when SNR = 20; it confirms the stability and practicability of the method.

6. Discussion and conclusion

A novel method for measuring pipeline thickness is proposed, which uses higher-order SH guided wave modes. Two sets of inversion formulas are derived based on the dispersion equation of SH guided waves with high-frequency approximation. The numerical simulation results for the specific examples considered in this study indicate that the proposed method can estimate the local wall thickness of both metallic and non-metallic pipelines without prior knowledge of their shear wave velocity. This evaluation method exhibits universality and high accuracy across different materials.

Earlier methods have been proposed to measure the local thickness of pipelines, providing detailed quantitative analysis, including defect location and accurate imaging using bulk waves at specific locations. While our proposed method cannot determine the size and location of damage at a specific spot between the transmitter and receivers, it can calculate the average thickness of the region between the transducers. Therefore, it can replace multiple measurements using bulk waves at various spots. The monitoring of changes in pipe wall thickness over a segment can be achieved by taking multiple readings over time, which is particularly advantageous for structural health monitoring. Nevertheless, it should be noted that this paper has some limitations; we did not consider whether this method can estimate wall thickness by obtaining adjacent dispersion curves in scenarios where guided waves are scattered and undergo mode transformation due to defects present in the material under investigation.

During production stages, most pipe materials are known and have similar shear wave velocities. Thus, questioning the significance of measuring shear wave velocity may arise. However, we believe that measuring this parameter is important, especially in cases involving unknown materials or chemical reactions due to pipeline corrosion, and impurities attached to the pipe wall. Even when material properties are known, the comparison of expected values with measured values remains beneficial for determining pipeline conditions. Dixon *et al.*[19] also presented a method for calculating sheet thickness using SH guided waves without prior knowledge of body wave velocity. His research focuses on calculation of the group velocity of a single higher-order mode (SH_1), specifically utilizing the dispersion curve of one mode. However, it was observed that there was a significant error when the thickness was less than 1.5 mm. In our paper, we proposed a method based on extracting two unknown modes' SH guided wave dispersion data points using two-dimensional Fourier transform to determine the thickness. This approach not only enables simultaneous calculation of the corresponding mode order, shear wave velocity, and thickness but also yields more accurate results across various thickness ranges. As an alternative to Dixon *et al.*'s technique,[20] we suggest employing low-frequency band-excited SH waves to obtain shear wave velocity and subsequently calculating pipe thickness from a specific higher-order dispersion curve. Although feasible, this alternative method undoubtedly adds complexity to detection work. In contrast, our proposed approach requires only a single excitation, significantly enhancing work efficiency.

Acknowledgements

Project supported by the Natural Science Foundation of Jilin Province of China (Grant Nos. 20240402081GH and 20220101012JC), the National Natural Science Foundation of China (Grant No. 42074139), and the State Key Laboratory of Acoustics, Chinese Academy of Sciences (Grant No. SKLA202308).

References

[1] Olisa S C, Khan M A and Starr A 2021 *Sensors* **21** 811
[2] Vogelaar B and Golombok M 2016 *Mechanical Systems and Signal Processing* **78** 107
[3] Lu D H, Cong G P and Li B 2022 *J Press Vess-T Asme* **144** 051801
[4] Simonov D, Vavilov V and Chulkov A 2020 *Sensor Review* **40** 283
[5] Nguyen L and Miro J V 2020 *IEEE Sensors Journal* **20** 14465
[6] Chen Y, Dong S, Zang Z, Ao C, Liu H, Gao M, Ma S, Zhang E and Cao J 2021 *Ocean Engineering* **234** 108865
[7] Kiapasha Z, Yahaghi E, Mirzapour M, Monem S and Nekoei J 2020 *Journal of Nondestructive Evaluation* **39** 10
[8] Koodalil D, Rajagopal P and Balasubramaniam K 2021 *Ultrasonics* **114** 106429
[9] Zima B, Woloszyk K and Garbatov Y 2022 *Ocean Engineering* **253** 111318
[10] Li W B, Hu N and Deng M X 2021 *Ultrasonics* **113** 106356
[11] El Mountassir M, Yaacoubi S, Mourot G and Maquin D 2018 *Mechanical Systems and Signal Processing* **112** 61
[12] Wang X, Qin C and Liu J 2019 *Chinese Journal of Scientific Instrument* **40** 166
[13] Li Z, Jing L, Wang W, Lee P and Murch R 2018 *J. Acoust. Soc. Am.* **144** 2824
[14] Belanger P 2014 *Ultrasonics* **54** 1078
[15] De Castro Ribeiro M G, Kubrusly A C, Ayala H V H and Dixon S 2021 *IEEE Access* **9** 40836
[16] Thon A, Painchaud G, Le D A and Belanger P 2022 *NDT and E International* **128** 102631
[17] Cui H, Li B, Zhou L B and Liu W 2022 *Smart Materials and Structures* **31** 095018
[18] Sun H, Peng L, Lin J, Wang S, Zhao W and Huang S 2022 *IEEE Transactions on Industrial Informatics* **18** 3235
[19] Dixon S, Petcher P A, Fan Y, Maisey D and Nickolds P 2013 *J. Phys. D: Appl. Phys.* **46** 445502
[20] Wróblewski R and Stawiski B 2020 *Buildings* **10** 154
[21] Velichko A and Wilcox P D 2009 *J. Acoust. Soc. Am.* **125** 3623
[22] Zhaoa X and Rose J L 2004 *J. Acoust. Soc. Am.* **115** 1912
[23] Luo W, Zhao X and Rose J L 2005 *Journal of Pressure Vessel Technology* **127** 345
[24] Zhai G F and Li Y Q 2020 *Chin. Phys. B* **29** 054303
[25] Qiu H, Chen M and Li F 2022 *Mechanical Systems and Signal Processing* **165** 108390
[26] Nakamura N, Ogi H and Hirao M 2011 *Jpn. J. Appl. Phys.* **50** 07CH17
[27] Kubrusly A C, Freitas M A, Weid J P and Dixon S 2019 *NDT and E International* **101** 94
[28] Nakamura N, Ogi H and Hirao M 2013 *Jpn. J. Appl. Phys.* **52** 07HC14
[29] Kubrusly A C and Dixon S 2021 *Ultrasonics* **117** 106544
[30] Becerril García D and Cortés-Pérez J 2022 *Tunnelling and Underground Space Technology* **122** 104397
[31] Hu J, Duan J, Chen Z, Li H, Xie J and Chen H 2018 *Mechanical Systems and Signal Processing* **99** 702